Iğdır Üniversitesi Fen Bilimleri Enstitüsü Dergisi, 14(3), 1186-1199, 2024
Journal of the Institute of Science and Technology, 14(3), 1186-1199, 2024
ISSN: 2146-0574, eISSN: 2536-4618
Chemistry **DOI: 10.21597/jist.1467666**
Research Article
Received: 12.04.2024 **Accepted: 18.07.2024**

To Cite: Gören, K., Bağlan, M. & Yıldıko, Ü. (2024). Melanoma Cancer Evaluation with ADME and Molecular Docking Analysis, DFT Calculations of (E)-methyl 3-(1-(4-methoxybenzyl)-2,3-dioxoindolin-5-yl)-acrylate Molecule. *Journal of the Institute of Science and Technology*, 14(3), 1186-1199.

Melanoma Cancer Evaluation with ADME and Molecular Docking Analysis, DFT Calculations of (E)-methyl 3-(1-(4-methoxybenzyl)-2,3-dioxoindolin-5-yl)-acrylate Molecule

Kenan GÖREN[1*], Mehmet BAĞLAN[1], Ümit YILDIKO[2]

Highlights:
- DFT Optimizations
- Melanoma Cancer
- Isatin

Keywords:
- DFT
- Moleküler Docking
- MEP
- ADME
- NBO

ABSTRACT:

In this study, we performed HOMO-LUMO energy calculations, molecular electrostatic potential surface (MEPS), optimized molecular geometry using B3LYP, B3PW91 methods and 6-311G(d,p) basis set of the target molecule (E)-methyl 3-(1-(4-methoxybenzyl)-2,3-dioxoindolin-5-yl) acrylate (MMDA) that is an isatin derivative, nonlinear optics (NLO), NBO analysis to investigate the stability of the molecule as a function of both hyper-conjugative interactions, charge transfer within the molecule and charge delocalization, and Mulliken atomic charge structure were examined using the Gaussian 09 software, and the results were displayed. In this study, ADME analysis was performed to analyze the problem of our molecule finding application in the field, focusing on producing effective and harmless pharmacological drugs. Finally, molecular docking analysis of the examined compound on melanoma cancer were performed with two different enzymes (PDB:3OG7) and (PDB:5EG3), and docking scores and receptor models were given.

[1]Kenan GÖREN (**Orcid ID:** 0000-0001-5068-1762), [1]Mehmet BAĞLAN (**Orcid ID:** 0000-0002-7089-7111), Kafkas University, Department of Chemistry, Kars, Türkiye.

[2]Ümit YILDIKO (**Orcid ID:** 0000-0001-8627-9038), Kafkas University, Department of Bioengineering, Kars, Türkiye.

***Corresponding Author:** Kenan GÖREN, e-mail: kenangoren49@gmail.com

INTRODUCTION

Cancer is a genetic disorder involving abnormal cell growth that attacks and spreads to other body parts. Cancer is also the second most prevalent reason for cardiovascular illness in developed nations and the third most common cause in different countries (Gyamfi et al., 2022). The World Health Organization's 2014 Worldwide Cancer Survey states that throughout the next 20 years, there will be a 57% rise in cancer cases globally. 26 Million new instances of cancer and 17 million cancer-related deaths are expected to occur each year by 2030 (Torre et al., 2015). The projected rise will mostly result from population aging and expansion, and it will be highest in nations with low and medium levels of resources. Various isatin derivatives have multiple biological anticancer properties. Widely present endogenously in human and other mammalian tissues and fluids is isatin, an indole derivative most likely the consequence of the tryptophan metabolic pathway. Because of its adaptable molecular architecture, isatin is a great candidate for structural modification and derivatization (Teng et al., 2016). Various isatin derivatives have multiple biological properties, including antifungal, anticancer, and antidepressant properties. Isatin and its analogs have a broad spectrum of antimicrobial, antitumor, antiviral, anti-inflammatory, and antioxidant activities. Isatin-containing heterocycles can also act as inhibitors of apoptosis by targeting proteases, caspases, kinases, and extracellular signal-regulated protein kinase (ERK) (Guo, 2019).

Because of its quick development, high death rate, and spread to other areas of the body, particularly when it is discovered too late, melanoma is considered one of the most deadly types of skin cancer. Even though a great deal of new treatment options have been developed recently, late-stage melanoma cancer remains incurable (Umar et al., 2020). Resistance to these treatments arises from the cancer's heterogeneity, alternative pathways (signaling), and some severe side effects that reduce the effectiveness of the new medication (Kızılbey & Akdeste, 2013). Therefore, new and effective melanoma-targeting medications still need to be developed, even if patients with advanced-stage melanoma now have better and more accessible therapy alternatives. Many tactics are being used, such as seeking out and assessing more effective delivery methods for already-existing chemicals (Özlük et al., 2017).

Today, it is possible to know the possible chemical properties of even an unsynthesized molecule with calculation programs (Kloeden et al., 2012). However, to obtain the best match between computational programs and real values, it is necessary to compare experimental values with those obtained with synthesized molecules (Saraç, 2018). This will be a guide for examining the similar properties of similar molecules in the future. Using the calculation programs, Density Functional Theory (DFT) is used to optimize the molecules, examine their geometric properties, analyze their orbital structures, and obtain detailed information about electronic transitions (Gümüş et al., 2015).

In this study, we drew the (E)-methyl-3-(1-(4-methoxybenzyl)-2,3-dioxoindolin-5-yl) acrylate molecule (Teng et al., 2016) using the GaussView 6.0 drawing program. TD-DFT study is important in terms of the potential effect of chemical bonds in binding the enzyme in cancerous tissue in the docking interaction by making theoretical calculations of the potentially used molecule. B3LYP, B3PW91 methods and 6-311G(d,p) basis set were used for the bond angles, bond lengths, relative charges, HOMO-LUMO, MEPS, NLO, and NBO analyses of the molecule used in theoretical calculations. Finally, in our study, ADME analysis of the isatin derivative molecule was performed, and a molecular docking study was conducted for melanoma cancer.

MATERIALS AND METHODS

Using TD-DFT techniques, quantum computations were performed to determine of structural and chemical characteristics MMDA molecule. The molecule's chemical computations were determined using B3LYP, B3PW91 methods and 6-311G(d,p) basis set, and the Gaussian 09 package program (T. Michael J. Frisch, 2016). Drawn molecule data was displayed in GaussView 6.0. The Discovery Studio 2021 client was used to illustrate the placement study data. The SwissADME (http://www.swissadme.ch) online database was utilized for ADME assessment of the MMDA molecule, and the Origin 2019b 64-bit program was used to compare Mulliken charges to the graphic figure. The Maestro 11.8 version was applied in the molecular docking studies (Release 2019).

RESULTS AND DISCUSSION

Structure Details and Analysis

The MMDA molecule was optimized with the B3LYP, B3PW91 methods and 6-311G(d,p) basis set, using the Gaussian 09 (T. Michael J. Frisch), 2016 calculation program to analyze the molecular structure. The most stable and lowest energy state of a molecule is known as geometry optimization (Kenan et al., 2022). All parameters for the MMDA molecule have been shown in Table 1. There are very minor differences here between the B3LYP, B3PW91 methods and 6-311G(d,p) basis set. This optimized structure showed minimal potential energy. Two optimized basis sets of the MMDA molecule were examined by comparison. The aromatic ring's optimal bond lengths and bond angles are between the usual limits. For B3LYP, the C–C bond lengths range from 1.34 to 1.50 Å, for B3PW91 C–O bond lengths range from 1.24 to 1.43 Å; whereas the oxygen atom connected to the aromatic ring has a length of 1.32 Å. C–H bond lengths in the aromatic ring vary between 1.080 and 1.083 Å. The range of all C-C-C bond angles is between 109° and 128°. In the compound, the C-H angle is 108°-122°, while the C-C-O angle is 110°-126°. When the atoms were viewed as dihedral bonds in the Gaussian 09 (T. Michael J. Frisch) program, we observed that some dihedral angles have negative results in angle degrees, while others have positive values. The theoretical bond lengths obtained are compatible with the experimental numerical data in the literature (Bhavani et al., 2024; Elangovan & Sowrirajan).

Table 1. Theoretically Obtained Some Bond Lengths (Å) and Bond Angles (°) of the MMDA Molecule

Bond Lengths	B3LYP/ 6-311G(d,p)	B3PW91/ 6-311G(d,p)	Bond Lengths	B3LYP/ 6-311G(d,p)	B3PW91/ 6-311G(d,p)
C7-O1	1.43342	1.42613	**C15-O16**	1.28188	1.24048
O1-C2	1.36225	1.35622	**C14-C15**	1.48191	1.48054
C2-O4	1.21141	1.20986	**C14-O17**	1.23992	1.23972
C2-C3	1.46929	1.46652	**N13-C14**	1.42548	1.41281
C3-C5	1.34529	1.34415	**N13-C18**	1.43969	1.43486
C5-C6	1.45728	1.45399	**C18-C19**	1.50564	1.50129
C6-C12	1.40571	1.40291	**C22-O25**	1.32634	1.32339
C12-C11	1.38976	1.38829	**O25-C26**	1.44004	1.43087
C10-C11	1.41490	1.41244	**C5-H28**	1.08753	1.08866
C11-C15	1.46653	1.46268	**C18-H36**	1.09648	1.09701
Bond Angles	**B3LYP/ 6-311G(d,p)**	**B3PW91/ 6-311G(d,p)**	**Bond Angles**	**B3LYP/ 6-311G(d,p)**	**B3PW91/ 6-311G(d,p)**
C7-O1-C2	115.30024	115.02655	**C10-C11-C15**	109.75742	109.71399
O1-C1-C2	110.54813	110.57423	**C14-C15-O16**	126.53234	126.51923
C3-C5-C6	128.18155	128.13254	**C10-N13-C14**	110.18839	110.39041
C8-C6-C12	119.03662	119.12340	**N13-C14-O17**	119.49613	119.43590
C8-C9-C10	118.32570	118.22602	**N13-C18-C19**	111.28477	110.79092

Table 1 (Countined). Theoretically Obtained Some Bond Lengths (Å) and Bond Angles (°) of the MMDA Molecule

Planar Bond Angles	B3LYP/ 6-311G(d,p)	B3PW91/ 6-311G(d,p)	Planar Bond Angles	B3LYP/ 6-311G(d,p)	B3PW91/ 6-311G(d,p)
C7-O1-C2-C3	-179.92228	-179.92239	**C12-C11-C15-O16**	177.63836	1.57780
O1-C2-C3-C5	179.76898	179.70856	**O16-C15-C14-O17**	-3.49549	-3.49990
C3-O5-C6-C12	179.18264	178.95261	**N13-C18-C19-C20**	-137.39150	-136.48010
C6-C12-C11-C15	-49.21604	177.44926	**C21-C22-O25-C26**	177.89865	177.89918

Mulliken atomic charges

With the help of Mulliken analysis, the ionic and covalent character of the bonding in the structure can be questioned. Positive binding populations indicate binding, while negative values indicate anti-binding (Bağlan et al., 2023). As the population value approaches zero, the ionic character increases, and the population value of the ideal ionic bond is zero. As the population value grows in a positive direction, the covalency of the bond also increases. The fact that the atomic charges are different from zero indicates the presence of an ionic bond in addition to the existing bonding character. The most often used technique for population analysis is the Mulliken load distribution. The foundation of this technique is the linear combination of atomic orbitals to produce molecular orbitals. This distribution, however, does not accurately depict each element's electronegativity (Wang & Yao, 2017). In some extreme cases, it can give a negative population of electrons in an orbital or account for more than two electrons in an orbital. As a result, some qualitative predictions are made using Mulliken loads instead of statistically forecasting the outcomes of experiments (Arivazhagan et al., 2015). To calculate the atomic charges of the MMDA molecule, data using Mulliken density analysis using B3LYP, B3PW91 methods and 6-311G(d,p) basis set are given in Table 2. We observed that some C atoms are negative and some are positive. In mulliken analysis, the most negative atoms are O1, O4, N13, O16, O17, O25 due to their electronegativity. In Mulliken analysis, using the B3LYP/6-311G(d,p) method, a) Structure Optimization, b) Bond Lengths, c) Atomic Mass, d) Mulliken Charge have been given in Figure 1. Finally, in the Mulliken analysis, the mulliken charges of some C atoms in our compound were compared using the same methods as the graph in Figure 2.

Table 2. Mulliken Atomic Charges of the MMDA Molecule

ATOMS	B3LYP/ 6-311G(d,p)	B3PW91/ 6-311G(d,p)	ATOMS	B3LYP/ 6-311G(d,p)	B3PW91/ 6-311G(d,p)
C2	0.401	0.420	**O1**	-0.355	-0.361
C3	-0.179	-0.205	**O4**	-0.354	-0.362
C6	-0.100	-0.125	**N13**	-0.403	-0.432
C8	-0.041	-0.045	**O16**	-0.294	-0.308
C9	-0.076	-0.083	**O17**	-0.151	-0.154
C10	0.172	0.187	**O25**	-0.368	-0.374
C12	0.020	0.026	**H28**	0.133	0.146
C14	0.335	0.351	**H31**	0.111	0.126
C15	0.204	0.226	**H32**	0.111	0.123
C18	-0.075	-0.106	**H33**	0.112	0.124
C20	-0.076	-0.083	**H35**	0.154	0.176
C21	-0.099	-0.112	**H36**	0.138	0.156
C22	0.162	0.165	**H38**	0.108	0.121
C23	-0.146	-0.160	**H39**	0.106	0.121
C24	-0.047	-0.039	**H41**	0.121	0.133
C26	-0.126	-0.164	**H43**	0.115	0.131

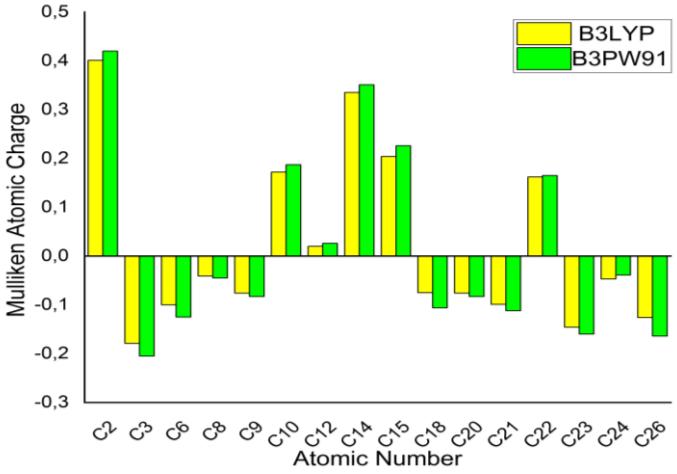

Figure 1. Mulliken Atomic Charge Comparison for the MMDA Molecule

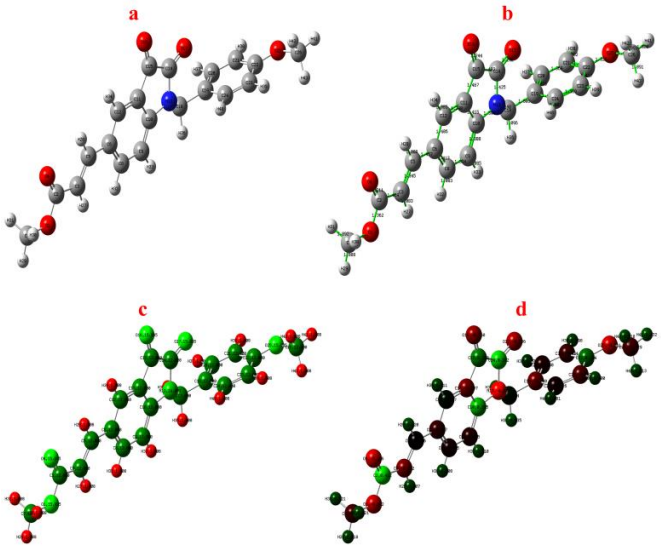

Figure 2. The MMDA Molecule with B3LYP/6-311G(d,p) Basis Set a) Structure Optimization, b) Bond Lengths, c) Atomic Mass, d) Mulliken Charge

HOMO and LUMO analysis

Frontier molecular orbitals (FMOs) are HOMOs and LUMOs. FMOs have a significant impact on quantum chemistry, UV-VIS spectra, optical, and electrical characteristics. The capacity to provide an electron is represented by HOMO, while the ability to receive an electron as an electron acceptor is represented by LUMO (Mehmet et al., 2023). A molecule's optical polarization, chemical hardness/softness, kinetic stability, and chemical reactivity are all determined by the energy gap between its HOMO and LUMO (Demir & Akman, 2017). The energy values of our compound's four primary molecular orbitals are as follows: B3LYP/6-311G(d,p) and B3PW91/6-311G(d,p) the lowest and second lowest empty MOs (LUMO and LUMO+1), and the second highest and highest occupied MOs (HOMO and HOMO-1). It is shown in Table 3 and was computed using TD-DFT. HOMO has an energy value of -5.5646 and -5.5741 eV, respectively, according to calculations. -3.5143 and -3.5679 eV, respectively, are the LUMOs. HOMO and LUMO have energy difference values of 2.0503 and 2.0062 eV, respectively. The last charge transfer interaction within the molecule, which influences the molecule's biological activity, is described by the HOMO-LUMO energy gap. In addition, the molecule becomes more stable, and the energy gap increases as it moves from the solvent phase to the gas phase. An electron density transfer is implied by the LUMO transition (Xavier & Gobinath, 2012).

The excitation of an electron from HOMO to LUMO is the primary characteristic of this electronic absorption, which reflects the change from the ground state to the first excited state. Consequently, the great electron-accepting capacity of the electron-accepting group leads to a substantial stabilization of the LUMO, which in turn causes a decrease in the HOMO-LUMO band gap. Figures 3 and 4 display the 3D graphs of the HOMO and LUMO orbitals for our compound that were estimated at the B3LYP/6-311G(d,p) and B3PW91/6-311G(d,p) levels.

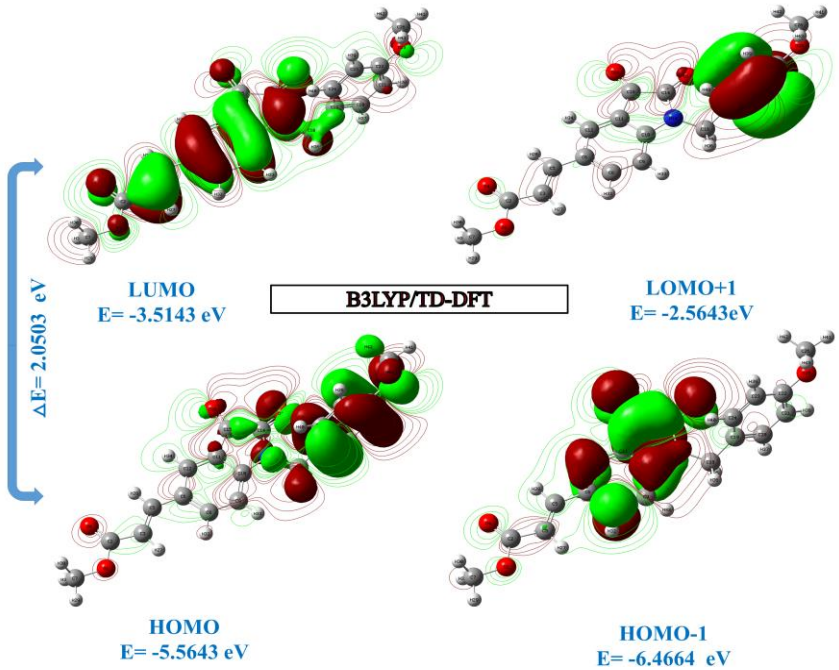

Figure 3. Boundary Molecular Orbitals of the MMDA Molecule According to the B3LYP/6-311G(d,p) Level

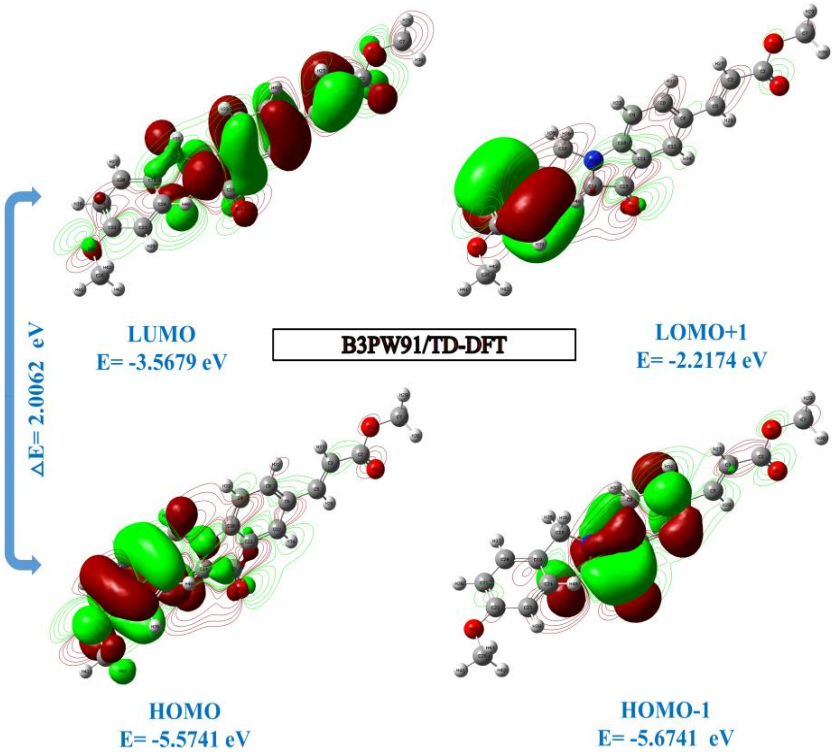

Figure 4. Boundary Molecular Orbitals of the MMDA Molecule According to the B3PW91/6-311G(d,p) Level

Table 3. Calculated Quantum Chemical Parameters*(in eV) for Low Energy Compatibilities by B3LYP/6-311G(d,p)- B3PW91/6-311G(d,p) Methods of the MMDA Molecule

Molecules Energy		B3LYP/ 6-311G(d,p)	B3PW91/ 6-311G(d,p)
E_{LUMO}		-3.5143	-3.5679
E_{HOMO}		-5.5646	-5.5741
E_{LUMO+1}		-2.1643	-2.2174
E_{HOMO-1}		-6.4664	-6.5447
Energy Gap	$(\Delta E)\lvert E_{HOMO}-E_{LUMO}\rvert$	2.0503	2.0062
Ionization Potential	$(I=-E_{HOMO})$	5.5646	5.5741
Electron Affinity	$(A=-E_{LUMO})$	3.5143	3.5679
Chemical hardness	$(\eta=(I-A)/2)$	1.0251	1.0031
Chemical softness	$(s=1/2\eta)$	0.5125	0.5015
Chemical Potential	$(\mu=-(I+A)/2)$	-4.5394	-4.5712
Electronegativity	$(\chi=(1+A)/2)$	2. 2571	2.2839
Electrophilicity index	$(\omega=\mu^2/2\eta)$	10.0508	10.4156

Molecular electrostatic potential (MEP)

Figure 5 in this work displays 3D graphs of the MMDA molecule's molecular electrostatic potential (MEP). Hydrogen bond sites and directions have been accurately predicted in some systems using MEP, a plot of the electrostatic potential projected onto a constant electron density surface. The total energy density is covered by the MEP surface. Since an approaching electrophile will be drawn to negative regions (where the electron scattering effect predominates), MEP is a helpful feature for evaluating reactivity. The maximum negative region in our compound is red, indicating a preference for signals of electrophilic assault, whereas the maximum positive region is blue, indicating a preference for signs of nucleophilic attack (Raju et al., 2015). As seen in Figure 5, the significance of MEP lies in its ability to concurrently display the molecule size, shape, and areas of positive, negative, and neutral electrostatic potential in terms of color gradation. This makes MEP an invaluable tool for examining the molecular structure in relation to its physiochemical structure. The resultant surface shows the electrostatic potential value as well as the size, shape, and size of the molecules concurrently (Ramalingam et al., 2012). Different hues correspond to different electrostatic potential levels on the surface. In this case, red denotes the highest repulsion and blue the strongest attraction.

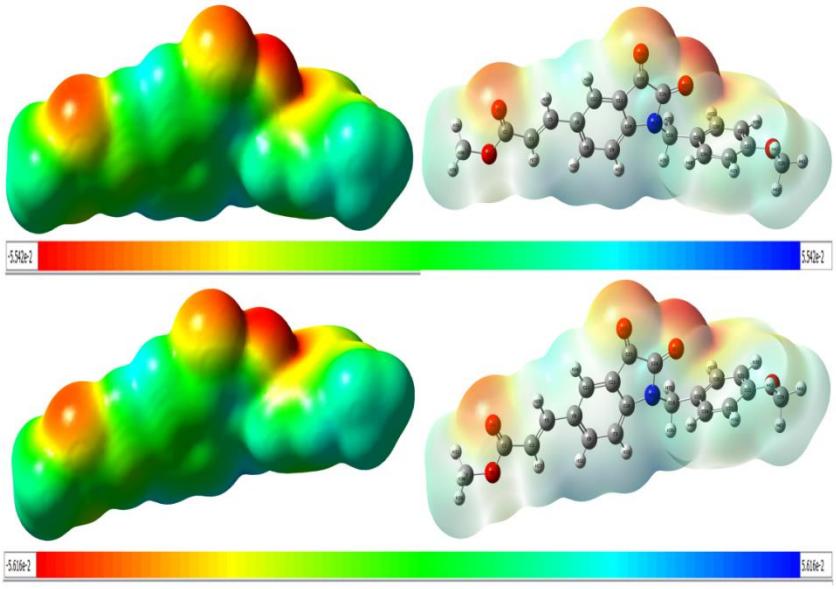

Figure 5. Molecular Electrostatic Potential Surface of the MMDA Molecule Using B3LYP/6-311G(d,p) and B3PW91/6-311G(d,p) Approximation and Basis Sets

Non-linear optical properties (NLO)

Compared to more conventional inorganic materials, organic materials have demonstrated improved second-order nonlinear optical characteristics in recent years (Shokr et al., 2022). This characteristic has drawn a lot of research interest in organic nonlinear optical (NLO) materials, together with the organic materials' many structural variants and intrinsic ultrafast reaction time (Khan et al., 2021). The finite field approximation was utilized to determine the second-order polarizability, also known as first hyperpolarizability (β), dipole moment (μ), and polarizability (α), using the B3LYP, B3PW91 methods and 6-311G(d,p) basis set. Using the x, y, and z components from the Gaussian 06W output, full equations 1-3 below were used to compute the average polarizability α, the β anisotropy of the polarizability, and the average first polarizability. Table 4 displays the hyperpolarizability β, dipole moment μ, and polarizability α. It was discovered that the computed dipole moment values were 4.3488 and 4.3101 Debye, respectively. The component with the largest dipole moment value is the μy component. Molecular hyperpolarization (β) in this molecule has been determined to be $2.44x10^{-30}$ and $2.70x10^{-30}$ esu, respectively. Molecular hyperpolarizability (β) magnitude is one of the critical elements of an NLO system.

$$\mu = (\mu_x^2 + \mu_z^2)^{1/2} \quad (1)$$

$$\beta_{Total} = (\beta^2 x + \beta^2 y + \beta^2 z)^{1/2} \quad (2)$$

$$= [(\beta xxx + \beta xyy + \beta xzz)^2 + (\beta yyy + \beta yxx + yzz)^2 + (\beta zzz + \beta zxx + \beta zyy)^2]^{\frac{1}{2}} \quad (3)$$

Table 4. The Dipole Moments (Debye), Polarizability (au), Components, and Total Value of the MMDA Molecule are Computed Using B3LYP, B3PW91 Methods and 6-311G(d,p) Basis Set

Parameters	B3LYP/ 6-311G(d,p)	B3PW91/ 6-311G(d,p)	Parameters	B3LYP/ 6-311G(d,p)	B3PW91/ 6-311G(d,p)
μ_x	-0.6437	-0.5890	**β_{XXX}**	-68.1296	-67.0998
μ_y	-4.2616	-4.3085	**β_{YYY}**	-60.9997	-62.2721
μ_z	-0.0255	-0.0455	**β_{ZZZ}**	-1.8166	-1.8888
$\mu_{(D)}$	4.3101	4.3488	**β_{XYY}**	4.6516	5.2480
α XX	-153.4995	-150.3677	**β_{XXY}**	-6.8049	-7.4862
α_{YY}	-155.2319	-153.3795	**β_{XXZ}**	5.4541	6.3762
α ZZ	-154.1727	-153.6725	**β_{XZZ}**	-9.8202	-9.5895
α_{XY}	15.5583	15.5416	**β_{YZZ}**	7.6692	7.4579
α_{XZ}	14.0293	14.3091	**β_{YYZ}**	4.2220	3.9121
α_{YZ}	4.4770	4.5252	**β_{XYZ}**	3.8967	4.2756
α (au)	-169.169	-165.8233	**β (esu)**	$2.44x10^{-30}$	$2.70x10^{-30}$

NBO analysis

The most accurate "Natural Lewis Structure" image is produced by NBO analysis because every orbital feature is mathematically selected to have the maximum percentage of electron density. The NBO method's ability to offer information about interactions in both virtual and occupied orbital spaces is a helpful feature that can enhance the investigation of intra, and intermolecular interactions (Weinhold et al., 2016). The NBO approach used the quadratic Fock matrix to assess donor-recipient interactions. The interactions lead to an empty non-Lewis orbital and the loss of occupancy of the localized NBO of the idealized Lewis structure (Zaboli & Raissi, 2015). The stabilization energy E(2) related to delocalization i→j for each donor (i) and acceptor (j) is given by, where F(i, j) is anticipated, εj and εi are diagonal elements, and qi is the donor orbital occupancy. The degree of conjugation of the entire system increases with a bigger value of E(2), indicating a stronger connection between electron donors and electron acceptors, or a greater propensity for donors to contribute to acceptors (Sakr et al., 2022). A stabilizing donor–acceptor interaction is represented by the delocalization of electron density between the occupied Lewis-type (bonding or lone pair) NBO orbital and the formally unoccupied

(antibonding) non-Lewis NBO orbital (Bouachrıne et al., 2021). NBO analysis was carried out on the molecule at the B3LYP/6-311G(d,p) level to clarify the intramolecular, rehybridization, and delocalization of electron density inside the molecule. The process of intramolecular contact takes place when the orbitals of π(C-C) and *π(C-C) bonds intersect. This leads to intramolecular charge transfer (ICT), which stabilizes the system. The relevant bonds in the C-C antibonding orbital are weakened by these interactions, which are manifested as a rise in electron density (ED). Table 5 clearly illustrates the significant stabilization energy of 25.49 kJ/mol and provides evidence of intramolecular charge transfer from (C2-C3) to *(C4-C5) antibonding orbitals. Furthermore, the charge distribution of all hydrogen atoms is the same, with the exception of hydrogen atoms H27, H28, H33, and H34.

Table 5. Selected NBO Results of the MMDA Molecule are Computed Using B3LYP/6-311G(d,p) Technique and Basis Set

NBO(i)	Type	Occupancies	NBO(j)	Type	Occupancies	E(2)[a] (Kcal/mol)	E (j)-E(i)[b] (a.u.)	F (i, j)[c] (a.u)
C2-C3	σ	1.97289	**C5-C6**	σ*	1.97238	4.67	1.16	0.066
C2-O4	σ	1.99613	**C3-C5**	σ*	1.97986	3.59	0.41	0.035
C3-C5	π	1.85634	**C2-O4**	π*	1.98489	20.92	0.30	0.073
C3-H27	σ	1.97862	**C5-H28**	σ*	1.97370	4.11	0.97	0.056
C5-H28	σ	1.97370	**C3-H27**	σ*	1.97862	5.54	0.95	0.065
C6-C8	π	1.59137	**C11-C12**	π*	1.64670	24.20	0.28	0.075
C6-C12	σ	1.97159	**C11-C15**	σ*	1.97257	4.33	1.14	0.063
C8-C9	σ	1.97453	**C10-N13**	σ*	1.98098	6.21	1.13	0.075
C9-C10	π	1.62454	**C6-C8**	π*	1.59137	24.75	0.29	0.076
C9-H33	σ	1.97749	**C10-C13**	σ*	1.98098	4.78	1.06	0.064
C10-C11	σ	1.95993	**N13-C18**	σ*	1.98121	4.94	1.05	0.064
C11-C12	π	1.64670	**C9-C10**	π*	1.62454	24.73	0.28	0.074
C11-C15	σ	1.97257	**C14-O17**	σ*	1.99430	4.18	1.23	0.064
C12-H34	σ	1.97875	**C10-C11**	σ*	1.95993	4.76	1.05	0.063
N13-C14	σ	1.98116	**C9-C10**	σ*	1.97472	4.45	1.33	0.069
C14-C15	σ	1.98144	**C11-C12**	σ*	1.97364	4.51	1.26	0.067
C14-O17	π	1.95884	**C15-O16**	π*	1.94332	7.43	0.37	0.048
C15-O16	π	1.94332	**C14-O17**	π*	1.95884	8.48	0.37	0.052
C18-H36	σ	1.96945	**N13-C14**	σ*	1.98116	4.44	0.88	0.057
C19-C20	σ	1.97214	**C19-C24**	σ*	1.65923	3.49	1.23	0.058
C19-C24	π	1.65923	**C20-C21**	π*	1.71432	20.69	0.28	0.069
C20-C21	π	1.97504	**C22-C23**	π*	1.64062	20.40	0.27	0.069
C20-H37	σ	1.97783	**C21-C22**	σ*	1.96942	4.14	1.05	0.059
C21-C22	σ	1.96942	**O25-C16**	σ*	1.99107	4.48	0.94	0.058
C21-H38	σ	1.97674	**C19-C20**	σ*	1.97214	4.33	1.07	0.061
C22-C23	π	1.97895	**C20-C21**	π*	1.71432	25.49	0.28	0.076
C23-C24	σ	1.97334	**C19-C24**	σ*	1.65923	4.29	1.26	0.066
C23-H40	σ	1.97777	**C19-C20**	σ*	1.97214	4.44	1.07	0.062

Molecular docking studies

Molecular docking studies facilitate the creation of novel, highly effective inhibitors by providing a complete understanding of the many interactions that occur between ligands and enzyme-active sites. The Maestro 11.8 version was applied in the molecular docking studies (Release 2019). The proteins responsible for melanoma cancer (PDB-CODE:3OG7) and (PDB-CODE:5EG3) were selected from the Protein Data Bank (http://www.rcsb.org) as protein receptors. The MMDA molecule was imported into Discovery Studio Visualizer, the hydrogen atoms were updated, and the extra water molecules in the X-ray structure were eliminated to create a PDB file. The MMDA molecule's binding affinity to the enzyme gave good results of -8.33 (PDB-CODE:3OG7) and -6.83 (PDB-CODE:5EG3) kcal, as shown in Table 6. This suggests that the chemical was intended to have anti-melanoma properties.

Tablo 6. Binding Scores (kcal/mol) of the Most Active Inhibitors in the Catalytic Domains of 3OG7 and 5EG3 Enzymes

Compound	Docking Score	
	(PDB: 3OG7)	(PDB: 5EG3)
The MMDA molecule	-8.33	-6.83

The 2D and 3D docking poses obtained from the Discovery Studio visualizer for the enzyme of the compound (PDB-CODE:3OG7) have been shown in Figure 6. As shown in Table 6 the MMDA molecule with a binding free energy of −8.33 kcal mol docks with the domain of the molecule. When the molecule-ligand interaction is evaluated, the strongest bindings are as follows: conventional hydrogen bonds SER-536 (3.95 Å) in the oxygen of methyl formate and CYS-532 (2.99 Å) in the oxygen of pyrrolidine, LYS-483 (4.59 Å) pi-cation bond in the benzene ring, HİS-539 (4.73 Å), VAL-471 (6.43 Å), ALA-481 (6.06 Å) and THR-529 (6.16 Å) pi-alkyl bonds, İLE-527 (5.46 Å) and LEU-505 (5.24 Å) alkyl bonds, PHE-583 (6.43 Å) pi-pi stacked bond in the pyrrolidine ring, İLE-463, GLY-593, PHE-595 and GLN-530 van der Waals bonds.

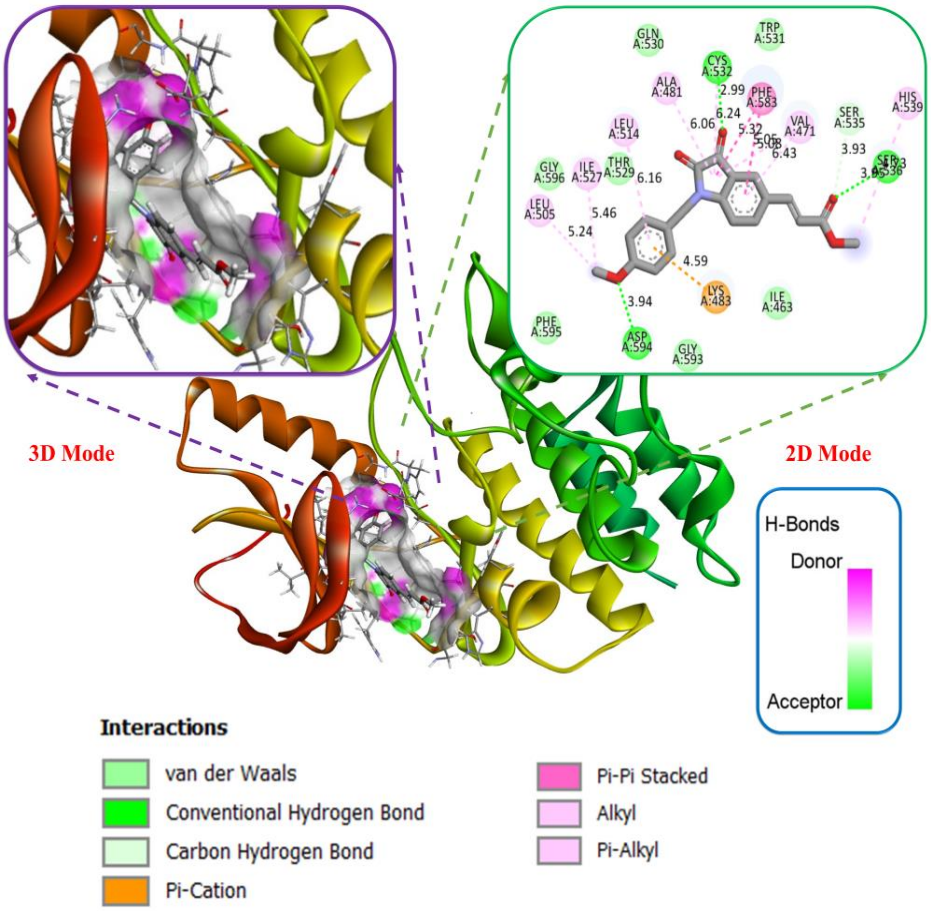

Figure 6. Ligand-3OG7 Mode of Interaction with Enzymes; 3D View of the Donor/Acceptor Surface of Hydrogen Bonds on the Receptor and 2D View of Ligand Enzyme Interactions

2D and 3D docking poses obtained from the Discovery Studio Visualizer for another enzyme of the compound (PDB-CODE:5EG3) are shown in Figure 7. As shown in Table 6, the MMDA molecule with a binding free energy of −8.33 kcal mol docks with the domain of the molecule. with a binding free energy of -6.83 kcal mol docks with the domain of the molecule. When the molecule-ligand interaction is evaluated, the strongest bindings are as follows: ARG-664 (6.14 Å) conventional hydrogen bonds in the oxygen of methyl formate, LYS-517 (5.53 Å) pi-cation bond in the benzene ring, LEU-633 (7.28 Å) and VAL-495 (4.28 Å) pi-alkyl bonds, LEU-519 (5.80 Å), ALA-515 (5.55 Å)

and LEU-487 (5.17 Å) alkyl bonds, LYS-517 (5.53 Å) metal acceptor bond in the pyrrolidine ring, ASP-527 (3.84 Å) carbon-hydrogen bond, ASP-530, ALA-491, ARG-630 and TYR-566 van der Waals bonds.

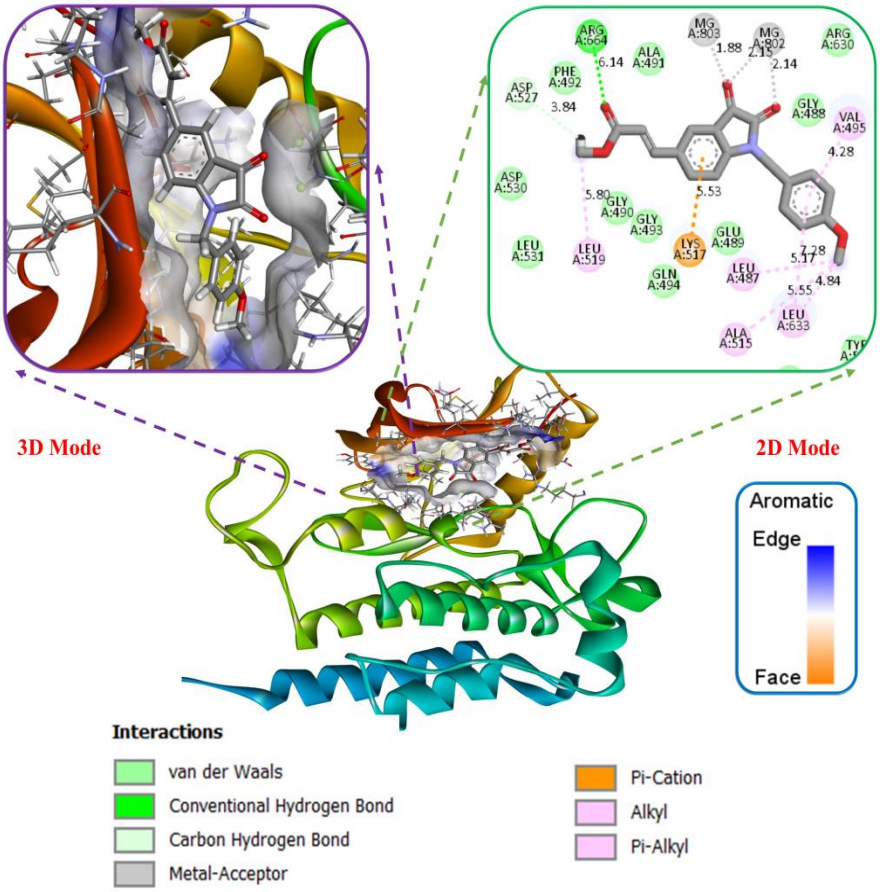

Figure 7. Molecule-5EG3 Mode of Interaction with Enzymes; a) 3D View of the Donor/Acceptor Surface of Aromatic Bonds on the Receptor b) 2D View of Ligand Enzyme Interactions

ADME analysis

The structural and physicochemical characteristics of the drug, such as its shape, lipophilicity, solubility, dissociation constant, protein binding, hydrogen bonding, and molar fractionation, greatly influence the degree of the ADME process (Sehout et al., 2021). A key factor that determines a drug candidate's usefulness and can significantly affect its pharmacokinetic characteristics is lipophilicity (Khodja et al., 2020). The connection between lipophilicity and pharmacokinetic characteristics has been explained by several studies. Because biological targets are lipid-based, there is a growing need for the creation of highly lipophilic medicines to attain the required selectivity and effectiveness of medications (Cetin et al., 2022). The Internet-based server SwissADME (http://www.swissadme.ch/index.php) was used to examine this ligand molecule's biological and chemo-informatic characteristics. Table 7 illustrates compliance with 91<140 requirements for Lipinski's MW 351.35 g/mol (<500), lipophilicity coefficient LogP 2.50 (≤ 5), H-acceptor 5 (≤ 5), H-bond donor 0 (<10), and Topological PSA 72. The physicochemical properties and color areas of the MMDA molecule are displayed in Figure 8. The polar surface area maps displayed in Figure 8 corroborate it. Red indicates polar regions, and gray indicates non-polar regions on TPSA maps. As a result, it is evident that when (1) and (2) change, the red-colored patches get progressively smaller.

Table 7. Physicochemical and Lipophilicity of the MMDA Molecule

Code	Lipophilicity consensus log P	Physico-chemical properties								
The MMDA		MW[a]g /mol	Heavy Atoms	Aromatic heavy atoms	Rot. bond	H-acceptor bond	H-donor bond	MR[b]	TPSA[c] (A^2)	% ABS[d]
	2.50	351.35	26	12	6	5	0	99.03	72.91	83.84

[a]**MW**, molecular weight; [c]**TPSA**, topological polar surface area; [b]**MR**, molar refractivity; [d]**ABS%:** absorption percent $ABS\% = 109 - [0.345 \times TPSA]$.

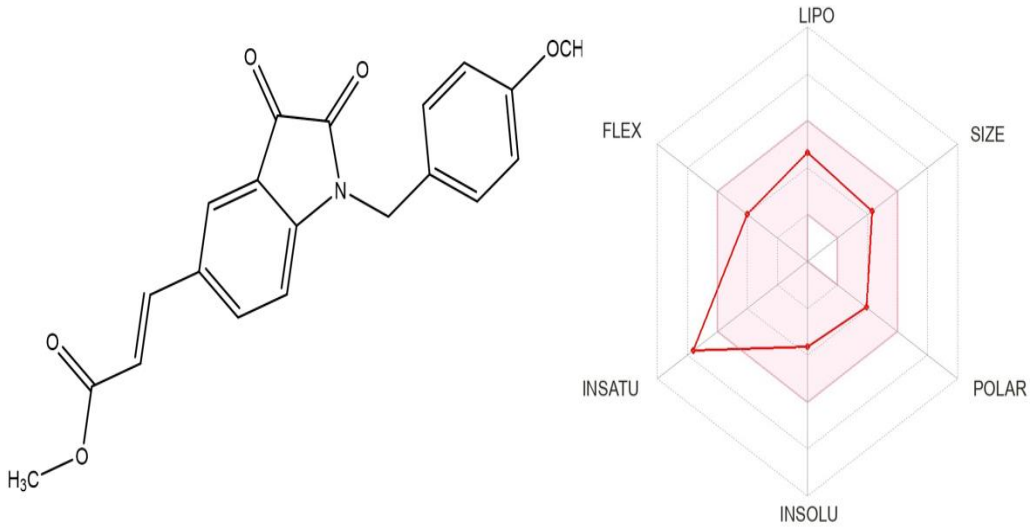

Figure 8. Color Regions and Physicochemical Parameters of the MMDA Molecule

CONCLUSION

In this study, theoretical calculations have been made for the MMDA molecule using the B3LYP, B3PW91 methods and 6-311G(d,p) basis set, and the theoretical calculation results have been reported. Structural theoretical calculations of bond lengths, bond angles and dihedral angles have been made using the B3LYP, B3PW91 methods and 6-311G(d,p) basis set. Following the theoretical calculations, NLO, MEP, HOMO-LUMO, Mulliken loads were calculated using the same method and basis sets. Using the same method and basis in theoretical calculations, polarite (α=-169.16 au and α=-165.8233 au) and static high-grade polarite (β=2.44x10^{-30} esu and β=2.70x10^{-30} esu) values were calculated. Additionally, ADME analysis was performed in our study, highlighting significant changes in TPSA and logPow values. It gave positive results for ADME analysis in accordance with Lipinski's rules. Finally, in our study, molecular docking analysis was performed to examine the specific binding position and ligand activity on the protein (PDB-CODE: 3OG7) and (PDB-CODE: 5EG3) responsible for melanoma cancer. To better understand inhibitory processes, binding approaches were investigated after determining the appropriate position for total ligand-enzyme docking. In the study, the shift scores in binding affinity with 3OG7 and 5EG3 were determined as -8.33 kcal/mol and -6.83 kcal/mol. In molecular docking analysis, we found that 3OG7 was more effective with a binding receptor score of -8.33 kcal/mol. Because this molecular structure has therapeutic potential, we believe that a new enzyme inhibitor option can be used to produce innovative drugs for melanoma cancer treatment.

Conflict of Interest

The article authors declare that there is no conflict of interest between them.

Author's Contributions

The authors declare that they have contributed equally to the article.

REFERENCES

Arivazhagan, M., Manivel, S., Jeyavijayan, S., & Meenakshi, R. (2015). Vibrational spectroscopic (FTIR and FT-Raman), first-order hyperpolarizablity, HOMO, LUMO, NBO, Mulliken charge analyses of 2-ethylimidazole based on Hartree–Fock and DFT calculations. Spectrochim Acta A Mol Biomol Spectrosc, *134*, 493-501.

Bağlan, M., Gören, K., & Yıldıko, Ü. (2023). HOMO–LUMO, NBO, NLO, MEP analysis and molecular docking using DFT calculations in DFPA molecule. Int. J. Chem. Technol, *7*(1), 38-47.

Bhavani, R., Kanagathara, N., Marchewka, M. K., Janczak, J., Senthilkumar, K., & Azam, M. (2024). Single crystal analysis and DFT studies of the novel hybrid material-based on 2-hydroxypyridine and selenic acid. *Results in Chemistry*, *7*, 101239.

Bouachrıne, M., Azaıd, A., Abram, T., Kacimi, R., Raftanı, M., Sbai, A., & Lakhlıfı, T. (2021). DFT/TDDFT studies of the structural, electronic, NBO and non-linear optical proper-ties of triphenylamine functionalized tetrathiafulvalene. J. Turkish chem. soc, *5*(2), 24-34.

Cetin, A., Toptas, M., & Türkan, F. (2022). Synthesis, biological evaluation, and bioinformatics analysis of indole analogs on AChE and GST activities. Med. Chem. Res., *31*(12), 2119-2131.

Demir, P., & Akman, F. (2017). Molecular structure, spectroscopic characterization, HOMO and LUMO analysis of PU and PCL grafted onto PEMA-co-PHEMA with DFT quantum chemical calculations. J. Mol. Struct., *1134*, 404-415.

Elangovan, N., & Sowrirajan, S. (2021). Synthesis, single crystal (XRD), Hirshfeld surface analysis, computational study (DFT) and molecular docking studies of (E)-4-((2-hydroxy-3,5-diiodobenzylidene)amino)-N-(pyrimidine)-2-yl) benzenesulfonamide. *Heliyon*, *7*(8), e07724.

Guo, H. (2019). Isatin derivatives and their anti-bacterial activities. Eur. J. Med, *164*, 678-688.

Gümüş, H. P., Tamer, Ö., Avcı, D., & Atalay, Y. (2015). 4-(Metoksimetil)-1, 6-dimetil-2-okso-1, 2-dihidropiridin-3-karbonitril molekülünün teorik olarak incelenmesi. *Sakarya University Journal of Science*, *19*(3), 303-311.

Gyamfi, J., Kim, J., & Choi, J. (2022). Cancer as a metabolic disorder. Int. J. Mol. Sci, *23*(3), 1155.

Kenan, G., Bağlan, M., & Çakmak, İ. (2022). Theoretical Investigation of ^{1}H and ^{13}C NMR Spectra of Diethanol Amine Dithiocarbamate RAFT Agent. TJST, *12*(3), 1677-1689.

Khan, A. U., Khera, R. A., Anjum, N., Shehzad, R. A., Iqbal, S., Ayub, K., & Iqbal, J. (2021). DFT study of superhalogen and superalkali doped graphitic carbon nitride and its non-linear optical properties. RSC Adv, *11*(14), 7779-7789.

Khodja, I. A., Boulebd, H., Bensouici, C., & Belfaitah, A. (2020). Design, synthesis, biological evaluation, molecular docking, DFT calculations and in silico ADME analysis of (benz) imidazole-hydrazone derivatives as promising antioxidant, antifungal, and anti-acetylcholinesterase agents. J. Mol. Struct, *1218*, 128527.

Kızılbey, K., & Akdeste, Z. M. (2013). Melanoma cancer. SIGMA J ENG NAT SCI, *31*(4), 555-569.

Kloeden, P. E., Platen, E., & Schurz, H. (2012). *Numerical solution of SDE through computer experiments*. Springer Sci. Rev.

Mehmet, B., Yıldıko, Ü., & Gören, K. (2023). DFT Calculatıons And Molecular Dockıng Study In 6-(2”-pyrrolıdınone-5”-yl)-(-) epıcatechın Molecule From Flavonoıds. *Eskişehir Teknik Üniversitesi Bilim ve Teknoloji Dergisi B-Teorik Bilimler*, *11*(1), 43-55.

Özlük, A. A., Oytun, M. G., & Günenç, D. (2017). Kanser immünoterapisi. *İstanbul Bilim Üniversitesi Florence Nightingale Transplantasyon Dergisi*, *2*(1), 21-23.

Raju, R., Panicker, C. Y., Nayak, P. S., Narayana, B., Sarojini, B., Van Alsenoy, C., & Al-Saadi, A. A. (2015). FT-IR, molecular structure, first order hyperpolarizability, MEP, HOMO and LUMO analysis and NBO analysis of 4-[(3-acetylphenyl) amino]-2-methylidene-4-oxobutanoic acid. *Spectrochim Acta A Mol Biomol Spectrosc*, *134*, 63-72.

Ramalingam, S., Karabacak, M., Periandy, S., Puviarasan, N., & Tanuja, D. (2012). Spectroscopic (infrared, Raman, UV and NMR) analysis, Gaussian hybrid computational investigation (MEP maps/HOMO and LUMO) on cyclohexanone oxime. *Spectrochim Acta A Mol Biomol Spectrosc*, *96*, 207-220.

Release, S., (2019). 3: Maestro Schrödinger. LLC, New York

Sakr, M. A., Sherbiny, F. F., & El-Etrawy, A.-A. S. (2022). Hydrazone-based materials; DFT, TD-DFT, NBO analysis, fukui function, MESP analysis, and solar cell applications. J. Fluoresc., *32*(5), 1857-1871.

Saraç, K. (2018). 4-Klorometil-6, 8-dimetilkumarin Bileşiğinin Sentezi ve Teorik Kimyasal Hesaplamaları. *Bitlis Eren Üniversitesi Fen Bilimleri Dergisi*, *7*(2), 311-319.

Sehout, I., Boulebd, H., Boulcina, R., Nemouchi, S., Bendjeddou, L., Bramki, A., Merazig, H., & Debache, A. (2021). Synthesis, crystal structure, Hirshfeld surface analysis, biological evaluation, DFT calculations, and in silico ADME analysis of 4-arylidene pyrazolone derivatives as promising antibacterial agents. J. Mol. Struct., *1229*, 129586.

Shokr, E. K., Kamel, M. S., Abdel-Ghany, H., Ali, M. A. E. A. A., & Abdou, A. (2022). Synthesis, characterization, and DFT study of linear and non-linear optical properties of some novel thieno [2, 3-b] thiophene azo dye derivatives. Mater. Chem. Phys, *290*, 126646.

T. Michael J. Frisch, G. W., Bernhard Schlegel, Gustavo Scuseria. (2016). (Version In Revision E.01)

Teng, Y.-O., Zhao, H.-Y., Wang, J., Liu, H., Gao, M.-L., Zhou, Y., Han, K.-L., Fan, Z.-C., Zhang, Y.-M., & Sun, H. (2016). Synthesis and anti-cancer activity evaluation of 5-(2-carboxyethenyl)-isatin derivatives. *Eur. J. Med. Chem*, *112*, 145-156.

Torre, L. A., Bray, F., Siegel, R. L., Ferlay, J., Lortet-Tieulent, J., & Jemal, A. (2015). Global cancer statistics, 2012. *CA: CA Cancer J*, *65*(2), 87-108.

Umar, A. B., Uzairu, A., Shallangwa, G. A., & Uba, S. (2020). QSAR modelling and molecular docking studies for anti-cancer compounds against melanoma cell line SK-MEL-2. *Heliyon*, *6*(3).

Wang, X., & Yao, J. (2017). Improvement of the self-consistent-charge density-functional-tight-binding theory by a modified Mulliken charge. Theor. Chem. Acc, *136*(10), 124.

Weinhold, F., Landis, C., & Glendening, E. (2016). What is NBO analysis and how is it useful? Int Rev Phys Chem, *35*(3), 399-440.

Xavier, R. J., & Gobinath, E. (2012). FT-IR, FT-Raman, ab initio and DFT studies, HOMO–LUMO and NBO analysis of 3-amino-5-mercapto-1, 2, 4-triazole. *Spectrochimica Acta Part A: Molecular and Biomolecular Spectroscopy*, *86*, 242-251. *Molecular and Biomolecular Spectroscopy*

Zaboli, M., & Raissi, H. (2015). The analysis of electronic structures, adsorption properties, NBO, QTAIM and NMR parameters of the adsorbed hydrogen sulfide on various sites of the outer surface of aluminum phosphide nanotube: a DFT study. *Structural Chemistry*, *26*, 1059-1075.